Advances in Water Resources 71 (2014) 81–92

Contents lists available at ScienceDirect

Advances in Water Resources

journal homepage: www.elsevier.com/locate/advwatres

Numerical investigation of chaotic advection past a groyne based on laboratory flow experiment

Márton Zsugyel [a,*], Tamás Tél [b,1], János Józsa [c,2]

[a] MTA-BME Water Management Research Group, Műegyetem rkp. 3., H-1111 Budapest, Hungary
[b] Institute for Theoretical Physics, Eötvös University and MTA-ELTE Theoretical Physics Research Group, Pázmány Péter sétány 1/A, H-1117 Budapest, Hungary
[c] MTA-BME Water Management Research Group and Department of Hydraulic and Water Resources Engineering, Budapest University of Technology and Economics, Műegyetem rkp. 3., H-1111 Budapest, Hungary

ARTICLE INFO

Article history:
Received 26 July 2013
Received in revised form 14 May 2014
Accepted 2 June 2014
Available online 9 June 2014

Keywords:
Mixing
Groyne
Chaotic advection
Open flow
PTV
LCS

ABSTRACT

A laboratory flow past a groyne with complex hydrodynamics was investigated using surface Particle Tracking Velocimetry (PTV) technique for detecting chaotic features in fluvial mixing processes. In the reconstructed velocity field particles were deployed and tracked numerically in a Lagrangian way. Calculating some appropriate parameters (e.g. flushing times, finite-size Lyapunov exponent) originating from chaos theory, we are able to give a more detailed picture on surface mixing driven by aperiodic flows than traditional approaches, including the separation of sub-regions characterized by sharply different mixing efficiency.

1. Introduction

Groynes are cross-wise built river training works for narrowing the river. The decrease of the cross-sectional area results in enhancing velocity, hence sediment deposition is less effective at the particular river reach. A very detailed study on the effects of groynes can be found e.g. in [1]. Although the main reason for building groynes is generally to maintain the navigation routes, other implications are also essential.

Material exchange processes in the vicinity of groynes are crucial for ecological habitats since the developed flow structure and resultant mixing might be advantageous for the fish, plankton species, and other organisms living in water. Since nutrients can be accumulated in the recirculation area, this region is also ideal for juvenile fish. That is why even ecological issues can be handled by a proper shaping of groynes [2]. Pollutants can also stagnate and be accumulated in the recirculation zone of groynes, which can then result in ecological deterioration there. The examples and problems provided above have been serious enough reasons for investigating river reaches containing one or more groynes. Research activities performed so far have focused mostly on the effect of the different groyne geometries on the flow [3], on the so-called exchange coefficient between the recirculation zone and the main flow [4,5] and also on certain ecological aspects related to the spatial distribution of phytoplankton in such an environment [6].

A span-wise obstacle causes, in general, a complicated flow field, as is also the case with groynes. High Reynolds number flows between two fluid bodies of different velocity are described as *turbulent free shear flows* (see e.g. [7]). Though Eulerian methods were extensively applied to this class of flows, it is hard to find anything about the Lagrangian description of the advection dynamics. In this paper we introduce some methods for characterizing mixing in river flows which are widely used already e.g. in oceanic [8] or in atmospheric applications [9].

Under natural circumstances, the flow around a groyne is persistent and non-stationary. The temporal dependence of the flow field is typically *aperiodic*. The flows, as all fluvial phenomena, fall under the category of *open flows*. In such cases, a fluid element will not return to large observational regions once it has left that region downstream. A third basic feature of the problem is due to the presence of up- and downwellings. As is known, the surface velocity field is thus *not divergence free*. The aim of this paper is

* Corresponding author. Tel.: +36 1 4631686.
E-mail addresses: zsugyel.marton@epito.bme.hu (M. Zsugyel), tel@general.elte.hu (T. Tél), jozsa.janos@epito.bme.hu (J. Józsa).
[1] Tel.: +36 1 3722524.
[2] Tel.: +36 1 4631496.

http://dx.doi.org/10.1016/j.advwatres.2014.06.004
0309-1708/

to investigate mixing processes mainly due to chaotic advection in groyne fields presenting such hydrodynamic features.

Chaotic advection has long been studied in both closed [10] and open flows [11] but most of the examples have been for two-dimensional, time periodic incompressible cases only. Less is known about advection in flows with temporally aperiodic, perhaps even chaotic, time dependence [12,13]. For a long time, chaotic advection in free surface flows has only been investigated under closed circumstances. It is only very recently [8,14] that such a process has been analyzed in open flow environment. Our paper attempts to provide a comprehensive study on the mixing dynamics in an experiment-based, aperiodic, open, free surface flow, with practical relevance in civil and environmental engineering.

In fact, despite the high number of valuable published investigations of fluvial mixing either in situ or in laboratory conditions, even if tracers and their various image processing-based analyses were used, they did not focus on revealing chaos and fractality in the phenomenon. These features are certainly not vital in river reaches with simple channel geometry where even the conventional Fickian approach can be applied, but in groyne zones they are definitely expected to bring novel insight and explanation to, e.g. the development mechanism of patchy or filamental features in tracer distribution, and consequently also in pollutant flushing or capturing characteristics. All this is of significant importance in aquatic environmental engineering at places where the protection of the quality of river water resources is a regular task. We are interested in mixing mainly on the surface, as a first approach, playing an important role in the case of floating type of pollutants of low enough density, often seen in nature due to, for example, non-treated outfalls and accidental spills. As surface processes are relatively easy to observe, they can be a reasonable target for implementing a novel approach. It might be interesting to note that the usefulness of this novel approach in the context of e.g. chemical and food industry was realized long ago. [15,16]

Our investigations are motivated by a recent field campaign in River Danube [17] in which GPS-equipped surface buoys, an essentially Lagrangian tool, were used to explore the dynamics of fluid elements in the vicinity of groynes. (A similar investigation was carried out by Sukhodolov et al. [18] in River Spree using surface tea candles in a nighttime video recording.) The trajectories and simultaneous positions of buoys drifted on the surface (for an example, see Fig. 1a) indicate rather strong deviations in spite of initially nearly identical locations, a qualitative indication of the chaoticity of the drifting process. A more detailed analysis of the data [17] also showed that by applying methods from chaos theory would substantially improve our ability to understand the behavior of pollutants in the spatially complex flow field at groynes. An example of this is given in Fig. 1b, where the distance between two of the three buoys is plotted as a function of time. The graph clearly indicates that the separation is exponential over a time interval of about 300 s. The rate of the exponential growth (turned out to be $\lambda = 0.004$ 1/s) is called the Lyapunov exponent and is known to be a quantitative measure of chaos [19]. The amount of obtainable field data is, however, limited by the low number of available buoys, rather expensive in themselves. A detailed Lagrangian analysis is thus not possible to perform based on field campaigns to date. That is why we decided for another setup.

A reasonable way to study the essence of the problem is to turn to laboratory scale and perform well controlled laboratory measurements. One has, of course, to keep in mind that a complete reproduction of the flow behavior found in the river is a hopeless task due to well known scale effects, nevertheless, preserving some key space-time flow features can result in spreading similar in character to that at the river scale. In such a laboratory flow it is then easy to substantially enhance the number of floating particles, and the trajectory of their drift motion as well as the drift velocity field itself can be reconstructed by an up-to-date method, e.g. Particle Tracking Velocimetry (PTV) [20]. As a simple setup, a single groyne scheme, a rectangular block orthogonal to the bank in a rectangular channel was implemented. Here a clear flow separation, a shear layer with vortex evolution, as well as, a large recirculation zone are present, all interacting with each other, and expected to reveal chaos in surface advection processes. At the first sight, this experimental approach seems to offer a straightforward opportunity to investigate the Lagrangian features of the flow purely based on laboratory particle tracking. However, the weakness of the technique in identifying uninterrupted particle trajectories long enough for obtaining chaos features led us to track numerical particles in the PTV-reconstructed unsteady velocity field. As will be demonstrated in the paper, the primary goal to achieve is to prove the presence and robustness of complex mixing patterns by using tools available in chaos analyses, occasionally by adapting them to the given conditions. Tools and methods, after verification, will have the potential to be used in investigating more complex and realistic cases, such as various groyne shapes and groyne fields in diverse channel geometries.

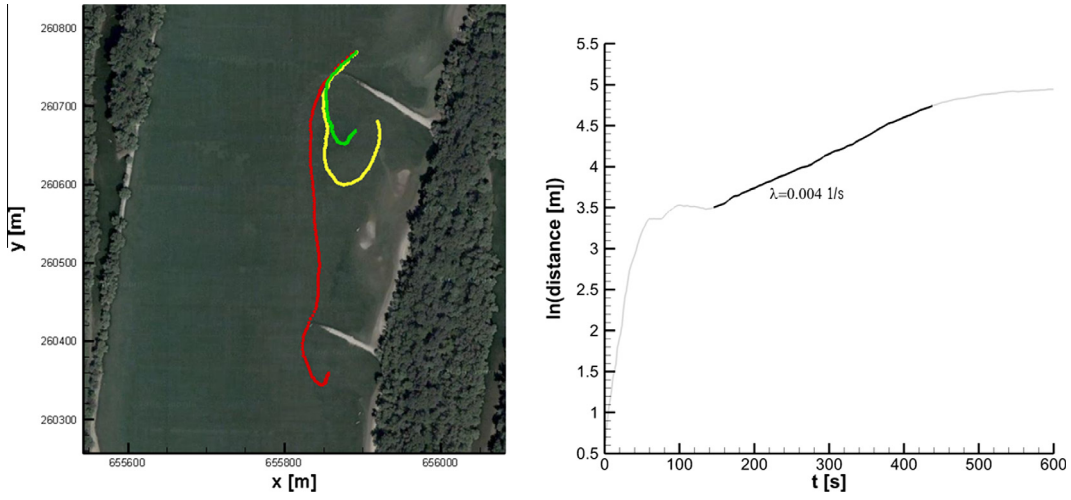

Fig. 1. Trajectories of three buoys followed for a time span of 26 min in the field of two groynes in River Danube initially released close to each other upstream of a groyne head (left panel). Plot of the distance between the red and yellow buoys vs. time in a log-linear representation. The marked linear section indicates exponential separation with a rate of 0.004 1/s (right panel). (For interpretation of the references to colour in this figure legend, the reader is referred to the web version of this article.)

The paper is organized as follows: in Section 2 we introduce our PTV-based laboratory measurements and the reconstruction of the velocity field. In Section 3 we present the scheme for numerical tracer advection based on the sequence of reconstructed velocity fields. Our results for the chaotic advection in the inherently unsteady shear zone are summarized in Section 4, including some general observations of the flushing time and escape rates, moreover, an analysis of the finite size Lyapunov exponent field. Lagrangian coherent structures, chaotic saddles and fractality are also discussed. The results are interpreted in terms of the theory of transient chaos and of random maps. Section 5 is devoted to the analysis of the recirculation zone. Finally, in Section 6 we summarize our conclusions.

2. Laboratory experiment to reconstruct the velocity field

The detailed analysis of a flow requires a large number of Lagrangian particles. The actual position of the particles at every time step has to be known in order to reconstruct the underlying velocity field. Such a large number of floating particles can be controlled in laboratory experiments, using PTV measurement technique, see e.g. [3].

The measurements were taken in a straight, rectangular open channel, which was 1 m wide and had a length of 8 m. A weir was built in at the outflow to control water depth (7 cm at the outlet section). The study area was selected in a 2.25 m long reach in the middle part of the channel, where a single groyne of size 30 cm times 5 cm with vertical edges for simplicity was placed as illustrated in Fig. 2. The typical stream-wise flow velocity upstream of the groyne was measured to be 0.05 m/s, which accelerated up to 0.1 m/s in the main stream passing the groyne. This velocity provides a Reynolds-number on the order of 7000 signifying turbulent flow; the Froude number is about 0.12.

In the measurements thousands of small, white polyethylene disks were released by manual seeding in this area. These markers had a diameter and thickness of 9 and 3 mm, respectively, and a density of $\rho = 0.97$ kg/dm^3. The number of floats, the location and the way of their deployment was chosen to provide an optimum number of particles in the test section: high enough to have a satisfactory coverage of the most important flow structures, but low enough to avoid significant particle interaction. After the floaters were spread in the flow – homogenously in the recirculation zone as well as upstream and downstream of the groyne in the main stream – the motion of the particles was recorded for around one minute by a CCD camera providing grayscale pictures of 1390×1040 pixel resolution at 30 Hz frequency. We count time from the instant of the first picture taken by the CCD camera.

Such recorded images are then in general processed with the PTV analysis algorithm in five major steps, according to [21]: (i) image pre-processing, (ii) particle detection, (iii) particle displacement determination, (iv) error filtering and (v) post-processing. Image pre-processing is to eliminate deceptive background elements on the images, e.g. bright pixels which might be identified as particles by the algorithms. Since in our case the background channel was black and therefore no false illuminating elements appeared, step (i) could be skipped. In step (ii) the so-called particle mask correlation method was used. After the setting of some geometric and intensity parameters, which were determined empirically for obtaining the best identification results, a reference particle mask was chosen. The used mask is then compared with every pixel on the image, and a cross-correlation map is calculated. A peak in this correlation map corresponds to the particle position. Using the Gaussian feature of the particle brightness, the intensity distribution of the centroid can be determined with sub-pixel accuracy. In the next step (iii) the used algorithm determines the particle displacements from the distribution pattern of the neighboring particles in the next time frame. Incorrect vectors may appear during the calculation because of, e.g. disappearing of particles. In step (iv) these erroneous vectors are filtered out. The used algorithm exploits the temporal similarity of the velocity vectors. Finally, since the obtained velocity field is spatially scattered, in step (v) we interpolate to an equidistant grid containing 200 and 100 nodes in the x and y direction, respectively, which corresponds to a spacing of about 1 cm. We note that the MATLAB scripts published in [21] were used for the PTV data processing.

To illustrate the compatibility of the measured and of the interpolated velocity fields we evaluated different measures. In the two panels of Fig. 3 the results of a point-wise comparison are shown for the whole measurement area. The left panel is the histogram of the angle differences between measured and interpolated velocities in intervals of 1°. The interval 0–1° is in fact the most likely one. It is also convincing to see the plot of the length of the interpolated velocities vs. that of the PTV-measured ones (right panel). The values scatter around a straight line of a slope very close to 1 with a large R^2 correlation coefficient. (The figures presented here belong to the starting time instant $t = 0$ s of the observation, we have checked, however, that they remain practically unchanged at later times.)

Moreover, the time-averaged velocity profiles were also compared with the experimental and numerical data of [22] along some particularly important transects around the groyne. A detailed presentation of the results is beyond the scope of this paper, but it is worth noting that satisfactory agreement was found.

Since the velocity data are extracted from those of plastic disks of 9 mm diameter, nearly identical to the grid spacing (1 cm), the result can only be interpreted as a flow field smoothed out on this scale. Small scale structures smaller than around 5 mm in radius are, thus, not resolved. The Lagrangian results are therefore not reliable on scales smaller than this. Interestingly, patterns much

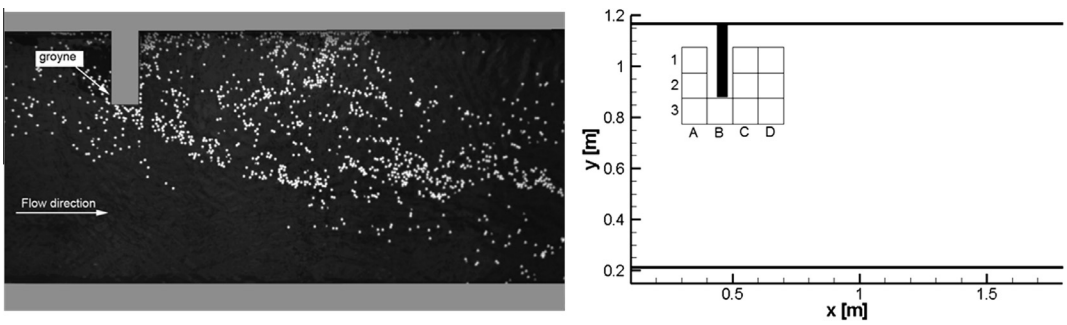

Fig. 2. Top view of the laboratory setup with the groyne and the marker particles for Particle Tracking Velocimetry (left panel). Schematic view of the groyne position in the channel including the cells out of which the tracer particles are released in the numerical simulations (right).

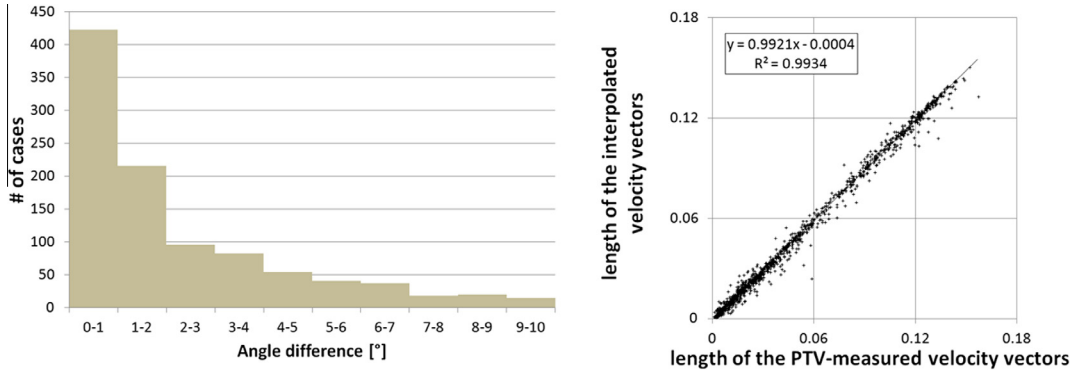

Fig. 3. Comparing the PTV-based and the interpolated velocity fields. Left panel: histogram of angle differences between the PTV measured and the interpolated flow field. Right panel: comparison of the velocity magnitudes.

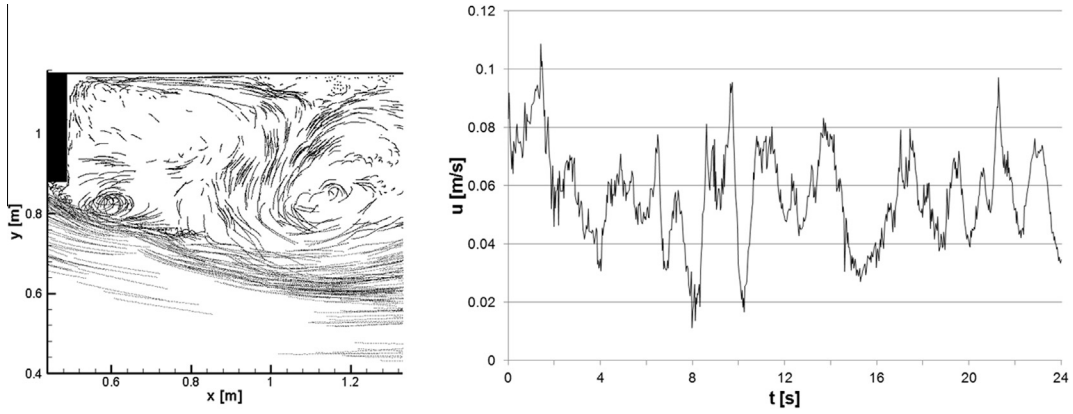

Fig. 4. PTV recorded particle paths over 2 s (left) and the Eulerian x-wise velocity component u over 24 s at the center point of cell B3 indicated in the right panel of Fig. 2 (x = 0.45 m, y = 0.825 m). A clear aperiodic behavior can be observed with an average period 3 s between the velocity peaks.

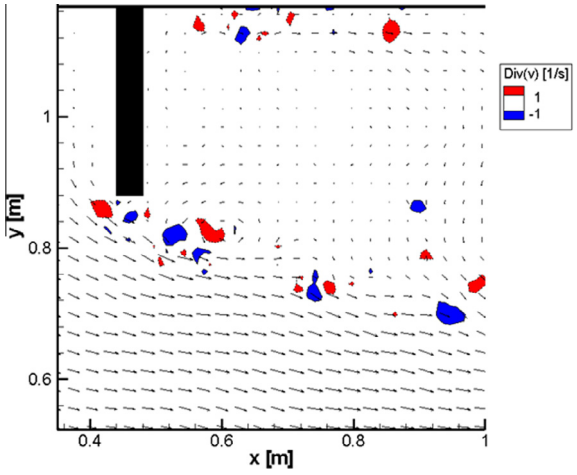

Fig. 5. A typical snapshot of the divergence of the reconstructed surface velocity field. The red and blue patches indicate instantaneous upwelling and downwelling regions, respectively (t = 1.3 s after the start of recording). (For interpretation of the references to colour in this figure legend, the reader is referred to the web version of this article.)

smaller than 5 mm do not appear in some of the figures (e.g. in Figs. 7a, 8c and d and in all panels of Fig. 10) illustrating a kind of consistency of the results. Where patterns on smaller scale appear like in Figs. 7b and 8a and b, these should be interpreted as mathematically created sub-grid features, only.

In the left panel of Fig. 4 one can identify (from bottom to top) the main Eulerian flow structures developing in the vicinity of an emergent groyne: vortices shedding from the groyne head lead to exchange processes in the shear layer present between the slow, essentially two-dimensional (2D) horizontal gyre in the recirculation zone behind the groyne and the main stream.

In addition to the velocity irregularities, the unsteadiness of the flow can also be observed: during this short recording time interval several particle trajectories crossed each other, a phenomenon that would have been impossible in a stationary flow. In the right panel the time series of velocity component u is shown in the centre point of cell B3, as reconstructed by PTV. It clearly indicates that the investigated flow is aperiodic.

Free surface flows provide a particular mechanism for attracting and repelling motion: upwelling and downwelling. These features, common in fluvial environments, convey material to and from the surface, therefore the surface flow velocity vector field in general is not divergence free as is seen in Fig. 5.

3. Trajectory simulations

A C++ code was developed to track particles numerically in the interpolated velocity field by a high accuracy Runge–Kutta method (RK) with Δt = 1/30 s, corresponding to the PTV camera frequency using bilinear planar interpolation. Numerical tracer particles were placed initially around the groyne in ten 0.1 m × 0.1 m cells (see Fig. 2) with 0.1 mm spacing. This implies a maximum number of ten million trajectory simulations, providing an appropriate amount to characterize the main Lagrangian features of the flow.

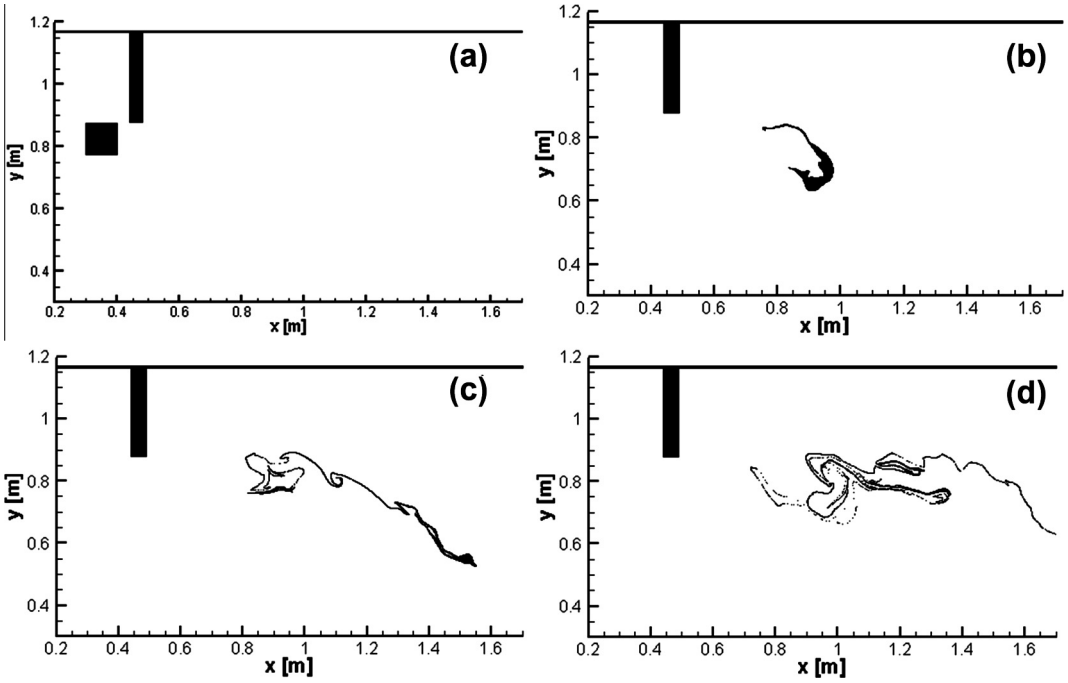

Fig. 6. Deformation of a square shaped surface dye droplet filling out cell A3 (black) at $t = 0$ s (a), 6 s (b), 12 s (c) and 18 s (d).

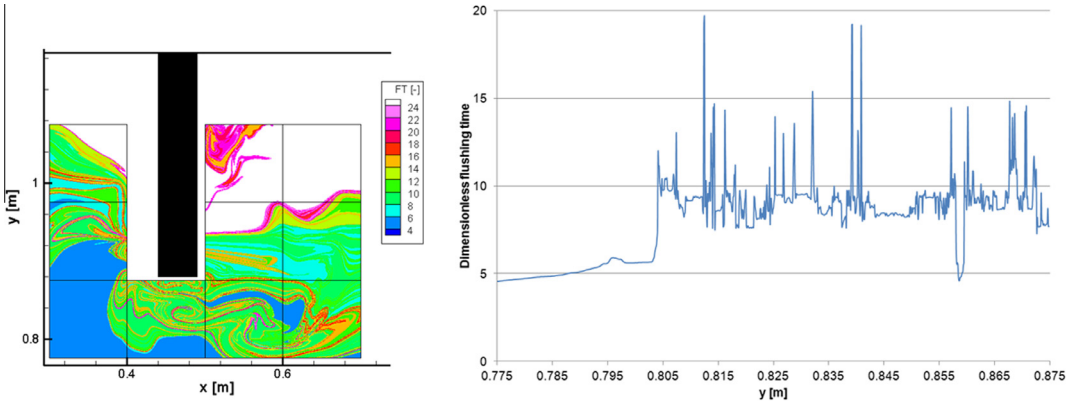

Fig. 7. Flushing times. Distribution of the flushing times measured in units of 3 s (of the time interval over which a fluid element in the main stream passes the length of the groyne) plotted over the cells of Fig. 2 with the values marked according to the color bar (left panel). Cross-sectional profile of this distribution at $x = 0.465$ m (within cell B3) (right panel). (For interpretation of the references to color in this figure legend, the reader is referred to the web version of this article.)

The solved equation was $d\mathbf{x}/dt = \mathbf{v}(\mathbf{x}, t)$, where the vector function $\mathbf{v}$ was approximated from the interpolated velocity field.

As a first acquaintance with the long term advection dynamics, let us monitor the fate of a surface floating dye droplet in the reconstructed flow field. We initiated $N = 10^6$ tracer particles uniformly distributed over cell A3 somewhat upstream of the groyne (Fig. 6a), and marked the positions of all the particles at fixed subsequent time instants. The droplet quickly becomes stretched and folded (Fig. 6b and c), and eventually forms a fine filamentary structure (Fig. 6d), while a part of it is flowing out of the range of observation.

4. Chaos characteristics

The strong deformation of the droplet is a clear indication of the chaoticity of the dynamics. Since, the flow becomes very complex in the study area, the particles undergo chaotic motion while flowing through (as it is typical in open flows). To characterize advection, we use methods worked out in the theory of transient chaos [23]. Novel features arising from the aperiodic time-dependence of the flow will be explained where necessary.

4.1. Flushing times

The time that a particle spends before reaching a suitably prescribed downstream border cross-section determines the flushing time of this particle. The flushing time distribution from a given region provides a measure of the irregularity of the tracer dynamics. To see this, we tracked trajectories until they reached the coordinate $x = 1.7$ m (corresponding to a downstream distance of $\Delta x = 1.2$ m, about 4 times the groyne length). Whenever this happened, the elapsed time was assigned to the initial position of the particle.

In a chaotic system the spatial distribution of the flushing time is filamentary because of the sensitivity to the initial conditions. Indeed, particles presenting short or long time to reach the border

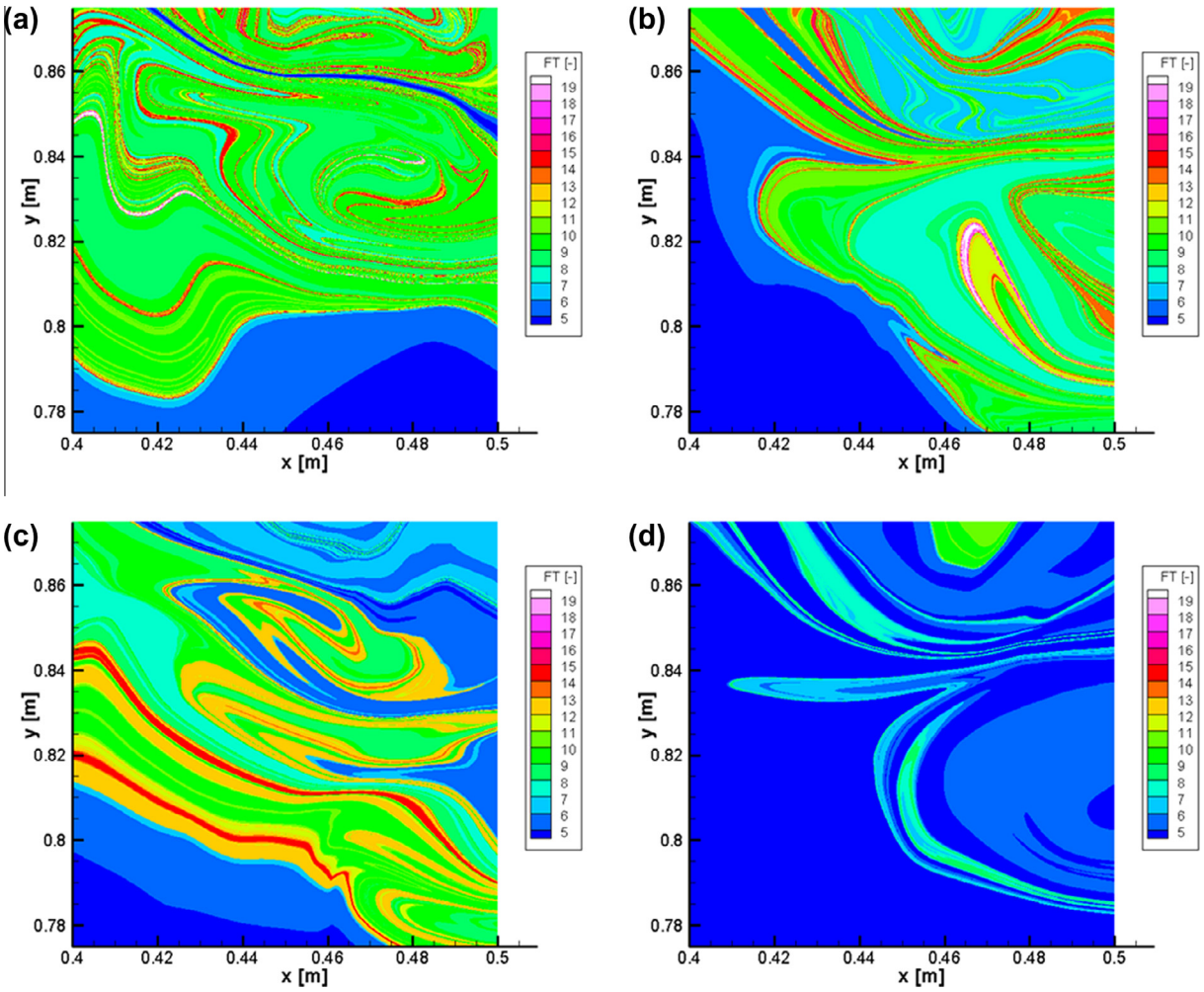

Fig. 8. Dependence of the dimensionless flushing time distribution in cell B3 near the groyne head on the starting time: $t = 0$ s (a), 3 s (b), 6 s (c), and 9 s (d).

cross-section might be very close to each other at the beginning of the observation.

A filamentary structure is indeed well visible in Fig. 7a. Regions marked with blue indicate short flushing time. Particles started from such places reach the border line very quickly. However, it is also remarkable that thin red filaments are enclosed in the well flushed areas. These structures correspond to a kind of stable manifold (for more details on the manifold and on its origin, the chaotic saddle, see Section 4.5), because these points stay for the longest time in the study area.

The dimensionless presentation (the time unit based on the groyne length $L = 30$ cm and on the typical flow velocity $U = 10$ cm/s is in the experiment $L/U = 3$ s) used in Fig. 7a enables us to project data for the original setup indicated in Fig. 1. As the largest lifetimes are about 20 dimensionless units, a similar case for River Danube, where the groyne length is about $L = 100$ m, the average flow speed is $U = 1$ m/s, and the natural time unit is $L/U = 100$ s, corresponds to largest lifetimes about 2000 s, i.e. 33 min in a range of 4 groyne length ($\sim$400 m) downstream of the groyne.

A Lagrangian interface line that separates the shear zone and the recirculation zone downstream of the groyne is also clearly visible as the boundary of the white region in cells C2–D1. White color marks areas from where the released particles do not reach the border line in the simulation period of 66.6 s. In Fig. 7b we present a typical y-wise cross-sectional profile of the flushing time distribution. This further confirms the fractal-like feature, and is analogous to the delay-time function of chaotic scattering processes [11,23].

Fig. 8 provides flushing time distributions with different starting time instants. In periodic flows the same pattern would be repeated with the period of the flow. In this aperiodic case, however, the pattern keeps changing with time, in principle forever. A theoretical background of chaotic advection in sustained aperiodic flows is provided by the theory of *random maps* worked out in [24]. It was successfully applied to the interpretation of the results of a closed free surface flow experiment [25], and extended to open flows [12,13,23]. A central statement of the theory is that patterns remains fractal forever, although the actual shape changes all the time. Another important feature of chaos is the rapid (exponential in time) separation of originally nearby trajectories (as also indicated by the buoy tracks of Fig. 1a and the data of Fig. 1b). The so-called average Lyapunov exponent is a global measure of this strong tendency for separation [19,26], i.e. for efficient mixing, in our hydrodynamic context. An interesting feature of sustained aperiodic flows is that chaos characteristics, e.g. the average Lyapunov exponent and corresponding fractal dimensions, are well defined and *independent* of time [23].

The results apply to flows that can be approximated as random perturbations of periodic ones (an assumption supported by Fig. 4 in our case). The key observation behind the statements is that all the members of an ensemble of tracer particles are subject to the *same local* random perturbation at any time instant.

The fact that the flushing time distribution remains fractal in time is also illustrated by Fig. 8. Note, that the different resolution of the spatial structures observed at different initial times is due to the decaying number of polyethylene disks from which the velocity vector field in the channel was reconstructed.

We emphasize that global flushing times from large regions (e.g. from cell D2) can easily be extracted from data of Fig. 7 left panel. By merely evaluating the arithmetical mean of the flushing times within a cell we obtain the results of Table 1 showing a remarkable difference of the global escape times between the shear zone and upstream regions. (Because the flushing times in the recirculation zone is much larger than the period of observation, cells A1, C1, D1 are not represented in Table 1.) Focusing on local flushing times instead of the global ones is decisive in our approach: the filamental patterns due to chaos enforce us to use a spatially refined scale description instead of a global one. This refined scale description requires the application of the novel tools to be outlined in Section 4.3–4.6.

4.2. Escape rates

In open flows a quantity characterizing the flushing process from a given region is the escape rate. The number $N(t)$ of survivors after time t decays for long time as

$$N(t) \sim \exp(-\kappa t) \tag{1}$$

where κ is the *escape rate*. The reciprocal of κ provides an estimate to the average flushing time (lifetime) of particles in the region of observation after the exponential decay sets in. Such a clear exponential behavior should be present in random maps as well, for sufficiently large particle ensembles. Since the particle number is unavoidably finite in our simulations, the decay appears with relatively large fluctuations. Nevertheless, an average exponential decay of $N(t)$ can be detected after a delay time t_0 which is about 22 s, that is about 7 time units (see Fig. 9). The negative slope of the ln N vs. t curve yields the escape rate. We investigated $N(t)$ in three different initial cells of Fig. 2 and found different escape rates (Fig. 9). In cell D3, close to the main stream, on which we concentrate now, the flushing is rather fast, and we find $\kappa_{D3} = 0.235$ 1/s. Thus, the average flushing time after t_0 is about 4 s, i.e. 1.3 dimensionless time units. (The same flushing time would imply 130 s in the main stream of River Danube). The two other initial cells, D2 and D1, are on the boundary of and inside the recirculation region, and hence are characterized by much smaller escape rates. We find in cell D2 $\kappa_{D2} = 0.070$ 1/s, consequently a flushing time approx. 15 s, that is 5 dimensionless units after t_0. The total flushing times $t_0 + 1/\kappa$ in cells D2 and D3 turn out to be good approximations to the global ones obtained as the means of the local flushing times in those cells (see Table 1). In cell D1, however, $\kappa_{D1} = 0.001$ 1/s (flushing time 1000 s, 330 dimensionless units after t_0), indicating indeed that typical flushing times are much longer there than the period of observation.

There are, however, large fluctuations around the fitted exponential decays. We note that in theoretical random maps the fluctuations disappear for very large particle numbers [13,23].

4.3. Finite size Lyapunov exponents

The particle separation is characterized traditionally by the average Lyapunov exponent, which is defined as the average exponential rate of separation of particles initially close to each other (see e.g. [26]). Aurell et al. introduced the concept of the finite size Lyapunov exponent (FSLE) as a generalization of this quantity [27,28]: at some time t particles are initiated around a point $\mathbf{x}$ on an equidistant grid with spacing δ_0, then they are tracked up to time τ, when the largest separation of their original edge neighbors reaches a specified threshold value δ_l. The FSLE is defined with the following formula:

$$\lambda(\mathbf{x}, t, \delta_0, \delta_l) = 1/\tau \ln(\delta_1/\delta_0). \tag{2}$$

This number is the larger the shorter the time is over which the initial small distance between two nearby particles expands to the predefined threshold distance. The FSLE can thus be considered to be a local measure of the mixing strength.

We determined the spatial distribution of the FSLE values assigned to the initial position of particle pairs at four different starting time instants. The results in Fig. 10 show strong filamentary structures, in all cases.

The overall pattern is similar to that of the flushing time distribution in the same cell (B3, see Fig. 8). Filaments marking larger FSLE values determine places where stronger particle separation occurs. Two significant ridges appear near the head of the groyne. Particles started on these (reddish) filaments are separated from their neighbors very fast. This indicates that (time-dependent) hyperbolic points are located somewhere in the flow. It is interesting to see also regions from where particles stay generally together in-between the well mixing filaments. Such regions are marked by white color. In these regions particle pairs either flow out of the region of observation before reaching the threshold distance or do not reach the threshold during the entire observation period of 66.6 s. The former is typical in this presented case, i.e. pairs do not separate more than 40 times their original distance over a typical flushing time which is at such places 12 time units. To see the drastic difference of the mixing strength to those within filaments, we mention that particles deviate from each other in the

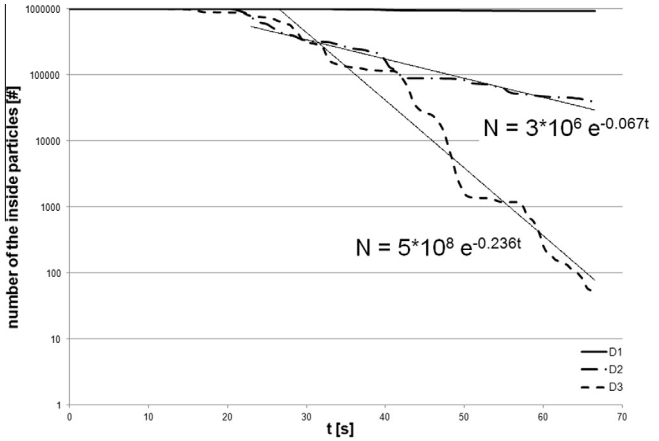

Fig. 9. The number of survivors in ($x < 1.7$ m) of an ensemble of $N = 10^6$ particles released in cell D3, D2, and D1 of Fig. 2. Thin continuous lines represent the fits of slope κ. The release from the recirculation zone D1 provides a rather straight graph with small slope, therefore we do not mark any fit there. The escape rate (the average slope after the delay time $t_0 = 22$ s, i.e. for $t > 22$ s) is largest close to the main stream (D3).

Table 1
Global flushing times characterizing the cells around the groyne edge (see Fig. 2 right panel).

Cell	A2	A3	B3	C2	C3	D2	D3
Dimensionless global flushing time [–]	8.0	5.7	8.7	13.3	9.0	10.3	9.7

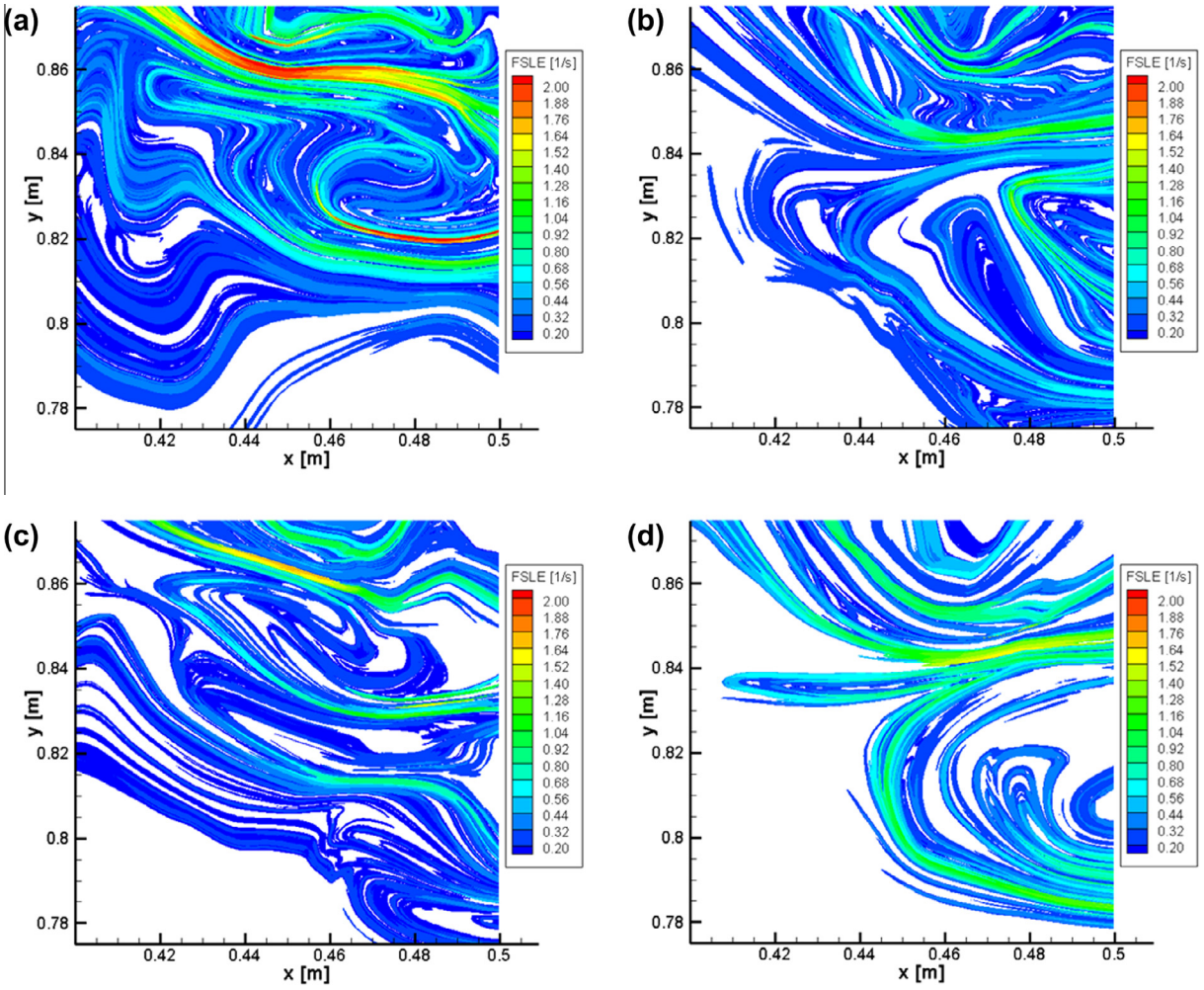

Fig. 10. Temporal evolution of the finite size Lyapunov exponent field in cell B3. Particles started from white regions stayed close together during the observational period (that is their FSLE is close to zero). Starting times are $t = 0$ s (a), 3 s (b), 6 s (c) and 9 s (d).

Table 2
The cell-averaged finite size Lyapunov exponent corresponding to different starting times in cell B3, the spatial distribution of which is shown in Fig. 10.

Initial time [s]	Average of FSLE [s^{-1}]
0	0.446
3	0.374
6	0.334
9	0.525
12	0.476

reddish region (where the FSLE value is 6 in dimensionless units) to more than 10^5 times their original distance over just 2 time units (6 s).

The filamentary FSLE patterns change in time without any repetition, in harmony with the random map theory. Their average over the same cell (presented in Table 2) appears to fluctuate over a mean value,

$$\lambda = 0.43\ 1/\mathrm{s},$$

that can be considered as an estimate of the average Lyapunov exponent over the chaotic transients.

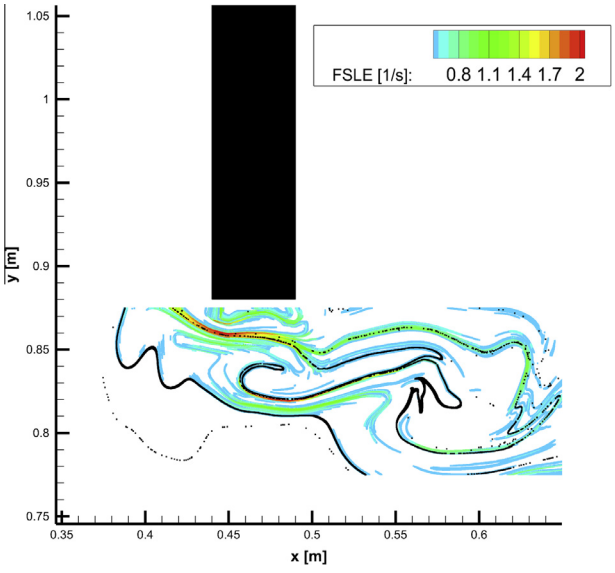

Fig. 11. Distribution of FSLE values in cells A3–D3 and flushing times only beyond the threshold value of 50 s are shown (black) and FSLE values only beyond the threshold value of 0.5 s^{-1} are colored.

4.4. Lagrangian coherent structures

The concept of Lagrangian coherent structures (LCSs) has been elaborated [29–33] to characterize transport in flows of arbitrary time dependence. It is therefore natural to briefly discuss these structures in our aperiodic flow. LCSs are special material filaments that prohibit fluid flux across themselves. They are thus also barriers to transport. The basic idea has recently been developed to investigate the strain, and the most repelling or attracting strain lines. Haller in [31] obtained rigorous results on the characterization of such material lines of aperiodic flows defined over finite intervals. It was pointed out that the analog of stable manifolds exists in the form of the most attracting strain lines. Intersections between the most repelling and attracting strain lines form so called hyperbolic cores, that are the analogs of hyperbolic orbits. Due to the finite-time observation of aperiodic flows, the LCSs are not unique, but they appear to be locally unique up to numerical precision for sufficiently long time intervals [31].

We have seen that a convenient measure to characterize the stretching dynamics is finite size Lyapunov exponents. It is expected that hyperbolic Lagrangian coherent structures are well approximated with maxima (ridges) of the finite size Lyapunov exponent fields [32].

In Fig. 11 we compare the ridges of FSLE with sets of large flushing times (black lines). The latter is obviously an LCS, since infinite flushing times can only belong to initial conditions hitting hyperbolic orbits, and initial conditions on the two sides of such lines deviate from these orbits in different directions. Fig. 11 illustrates that the curves of large flushing times (marked by black) coincide approximately with ridges of the FSLE field (for a more detailed recent theory, see [34]).

4.5. Chaotic saddle

The chaotic set underlying transient chaos is known to be a *chaotic saddle* (for an elementary presentation, see [26]). This is a non-attracting set that contains an infinity of unstable (hyperbolic) cycles. Since each cycle possesses a stable and an unstable manifold, the full chaotic saddle also has such a manifold. They are always fractal objects.

A more direct appearance of the manifolds, and of the saddle, can be seen in the sequence of Fig. 12. We start monitoring the

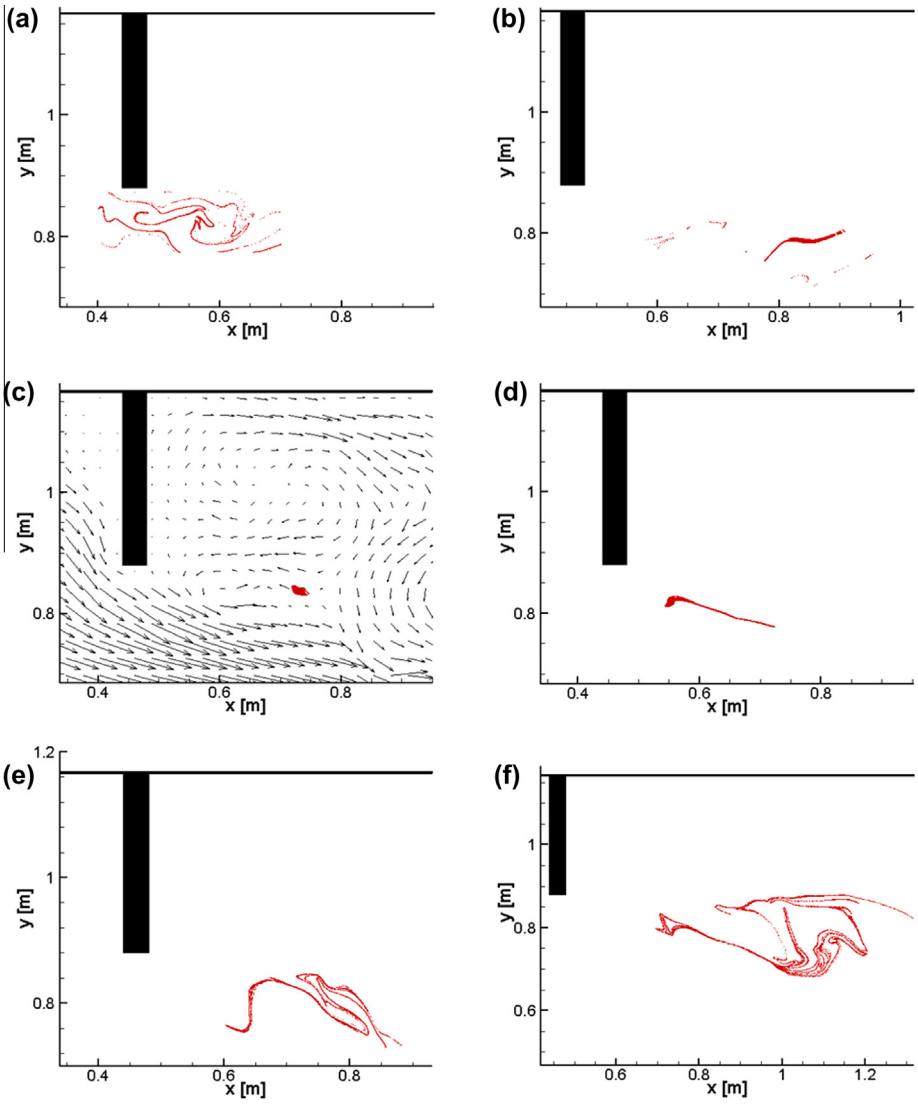

Fig. 12. Locations with flushing time values larger than 50 s correspond to a stable manifold. This filamentary manifold (a, $t = 0$, the same as the black line in Fig. 12) first converges (b, $t = 6$ s) to a time-dependent saddle (c, $t = 18$ s) later it is stretched (d, $t = 27$ s) and folded (e, $t = 36$ s) by the flow which results again in a fractal-like structure (f, $t = 45$ s).

points belonging to the large flushing time values in panel *a*. The convoluted, filamentary pattern becomes more compact (panel *b*), and appears to converge to a localized object (panel *c*). In a first approximation, this object might be interpreted as a (somewhat fuzzy) hyperbolic point. The presentation of the velocity vector field at this time instant shows, that this object is indeed close to an instantaneous stagnation point of the Eulerian flow. Somewhat later, the particles start to spread along a smooth line (as they should along the unstable manifold of a single hyperbolic point). Later on, however, as panels *e* and *f* indicate the set becomes more and more folded. This can only be explained by excluding the option of a single hyperbolic point. The localized object in panel *c* should contain many hyperbolic cycles. This object should be part of a (temporally ever changing) chaotic saddle. All filamentary objects seen up to now are related to the fractal manifold of such chaotic saddles.

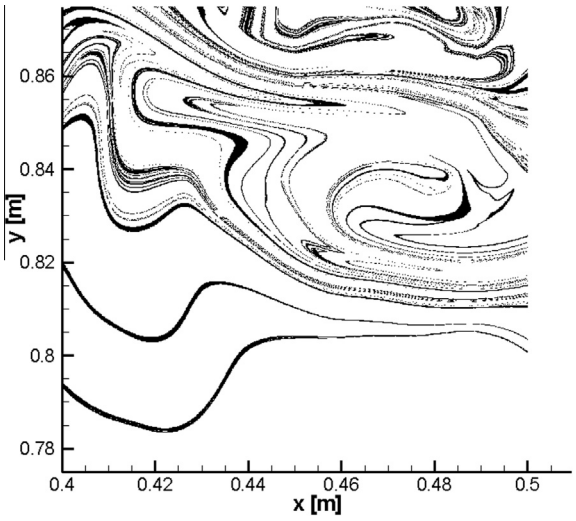

Fig. 13. Locations with flushing times (in cell B3) larger than 33 s. This set is a fractal of dimension $D_0 = 1.62$.

4.6. Fractal dimensions

In order to determine the fractal dimension, the box counting method (see e.g. [26]) was applied. Grids with different resolutions between 10^{-1} and 10^{-4} m were laid on flushing time values larger than a threshold. Then the log number of boxes containing at least one point was plotted vs. the log of the box size. The slope of this curve is the fractal (box counting) dimension. Experience showed that the half length of the whole measurement period (33 s) is an acceptable threshold, providing continuous filaments and a stable fractal dimension. In Fig. 13 points characterized by flushing times larger than this threshold are shown in cell B3. The calculated fractal dimension of this pattern is $D_0 = 1.62$.

It is worth mentioning that in a divergence free two-dimensional open flow, the information dimension of the stable manifold (corresponding to locations with large flushing time values) would be expressible [23] as

$$D_1 = 2 - \kappa/\lambda. \tag{3}$$

This expression is shown to hold in random flows, too [12,13]. Given that the information dimension is typically close to (but smaller than) the fractal dimension, we would expect $D_1 \approx D_0$. With the estimated κ and λ values ($\kappa_{B3} = 0.235$ 1/s and $\lambda = 0.43$ 1/s) the quantity $2 - \kappa/\lambda$ is about 1.63. Such a good agreement has been found with patterns taken at other initial times, too.

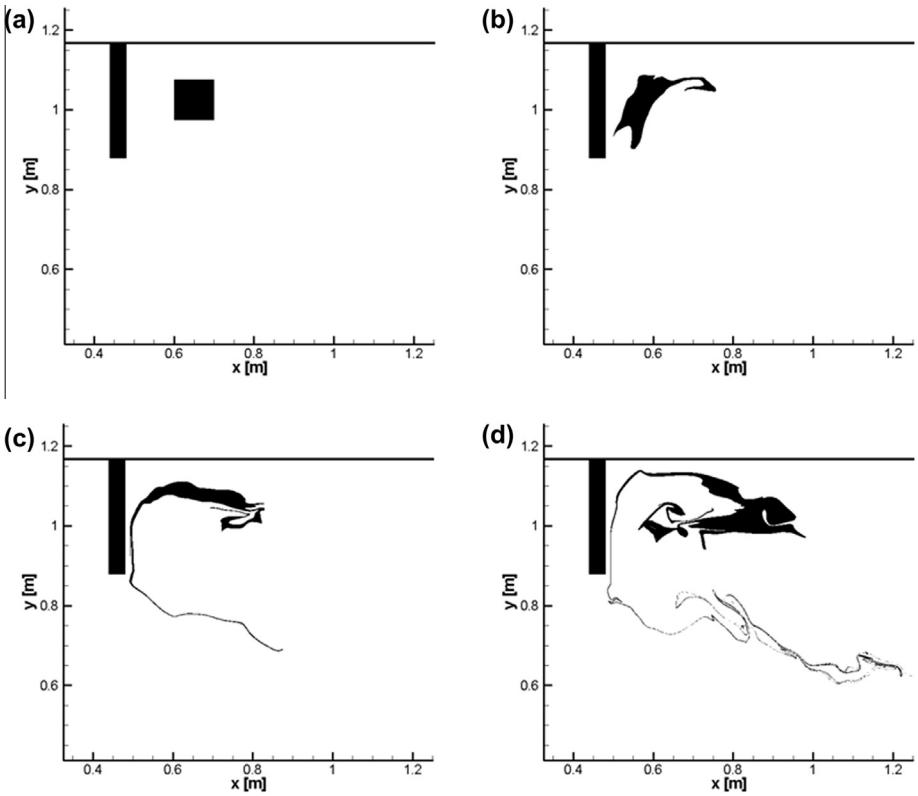

Fig. 14. Deformation of a square-shaped surface dye droplet of $N = 10^6$ particles (black) started within cell D1 downstream of the groyne at $t = 0$ s (a). The shape of the droplet at $t = 12$ s (b), 24 s (c), and 36 s (d).

5. The recirculation zone

As mentioned in the Introduction, the knowledge of the mixing properties in the recirculation zone behind the groyne is crucial for ecological issues since both nutrients and pollutants might accumulate in this area. Earlier studies aimed at unfolding the dynamical structure of this zone and its impact on the (Eulerian) exchange rate with the main stream (e.g. [35]). For multiple-groyne setup it was found that, depending on the geometry, one or two gyres are formed in the zone between groynes. In our single-groyne case, however, the gyre pattern is different. In instantaneous velocity fields a complicated picture can be observed: some smaller vortices freshly shed from the shear zone influence the flushing processes as they carry particles away from and take others back into the recirculation zone (see e.g. Fig. 4, left panel). Though the mass transport between the main flow and the recirculation zone is enhanced by the vortices developing in the shear layer, the flushing time is still large in most of the recirculation zone, implying slow dilution there.

In Fig. 14 we present how a surface dye droplet consisting of 10^6 numerical particles, released from the recirculation zone in cell D1, is advected. The initial shape seen in panel *a* starts to deform so, that two narrow filaments are stretched out from the lower part towards the groyne head, whereas the upper region of the dye moves towards the wall (panel *b*). In panel *c* a thin filament is observable, along which some particles have already left the recirculation zone, but most of them remain still trapped in the gyre. In the last panel the shedding vortices have already folded the escaping particle filaments many times, while the particles released initially in the upper part of the droplet start to fill the gyre.

In dynamical systems terms, the recirculation zone contains in time-periodic flows a KAM torus, which plays the role of a separatrix, separating a region of never flushing fluid from the main stream. The escape rate for this region is then exactly zero. The fact that in our aperiodic flow flushing (even if very weak, see Fig. 9, line marked as D1) takes place, shows that such an exact separatrix does not exist. This is in harmony with the statement of the random map theory [12] according to which no KAM tori can exist in random flows. Aperiodic time dependence leads here to a strong separation of the time scales characterizing the mean stream and the recirculation zone.

6. Conclusions

Before summarizing the essence of our approach, we present a situation different from the one related to groyne fields where methods similar to the ones used in the paper could successfully be applied.

Free shear layers dominate river junctions whenever the two streams arrive there at different flow speeds. Due to the differences in suspended solids content their structure and evolution often become visible. Such a case is given in Fig. 15a showing the junction of two medium size rivers in Hungary. In fact, the sharp contrast in the water color is linked to the breaching of a red mud deposit dam well in the upstream catchment part of one of the rivers (occurred in October 2010, cf. in [36]). The mud spillage unfortunately reached the river but was on its way effectively neutralized by using large amounts of plaster powder. Such a grayish plume reached then the junction region making the shear layer exceptionally visible. What can be seen there is a Kelvin–Helmholtz type vortex evolution with strong two-dimensionality, resulting in more and more stretched interface.

As a more recent event at the same site, a floating algae plume released from an upstream sidearm made some additional flow and resulting mixing patterns visible and worth for further study. In Fig. 15b one can easily observe the effect of coherent three-dimensional structures on the surface mixing. The eddies, though inherently three-dimensional by nature tend toward two-dimensionality in their turbulent features as reaching the surface. The eddies as well as the resultant succession of upwelling and downwelling zones make then the algae pattern very patchy and strongly filamental, both requiring further analysis to obtain quantitative mixing parameters, most likely with fractal features in them. All the methods presented in the bulk of the paper originated from the inherent fractal nature of mixing in free shear flows and are, therefore, applicable to the above mentioned examples as well.

Fig. 15. The confluence of Rivers Rába and Mosoni-Duna in Győr on 8/10/2010 (left) and fractal-like algae filaments drifted by the stream in the same confluence on 5/9/2013 (right).

Our aim in the paper was to demonstrate the ubiquitous fractal nature of mixing and its various implications on the behavior of floating pollutants drifted on the surface. The quantified and analyzed chaos characteristics all shed light on the basically same phenomenon, making it easier to understand and interpret for practical applications. In fact, for engineers dealing with river water quality issues, affected from time to time by severe pollution, a reasonable knowledge of the mixing features discussed in the present paper can upgrade planning, prevention, as well as remediation skills. At a later, more developed stage this knowledge could be applied not only to evaluate existing groyne configurations built exclusively for classical river training purposes, but also to modulate the planning of new ones, reconciling the often conflicting aspects of e.g. fluvial navigation-related river training measures, environmental protection and even ecological habitat conditions. In doing so,

- the novel details demonstrated on flushing time and escape rate irregularities, going even down to filamental patterns are essential to see hydrodynamics-driven cleaning up,
- or on the opposite, occasionally unacceptably long stagnation, distinguished all that for the main stream, the shear and the recirculation zones.
- Lyapunov exponent distributions traditional in revealing chaos in particle separation, a possible measure of mixing strength, gave patterns similar to the one of flushing time, thus supporting the coexistence of exponential particle separation and of extremely short flushing times, nearby.
- Further on, the revealed features and mechanisms were then put in the general context of Lagrangian coherence structures, and
- also in a more detailed discussion of the vital role of chaotic saddles.
- Finally, fractality found in the flushing time patterns were even quantified, with its dimension defined by a simple theoretical formula for characterizing the stable manifold (locating large flushing time values).

They all mean novel scientific achievements having at the same time strong relationship to immediate practical application. In fact, being experienced with the uncertainty and sensitivity of the fate of individual pollutants provides very up-to-date skills for practicing engineers in fluvial water resources protection and management.

Acknowledgements

Support to this work has been received from Hungarian Scientific Research Fund (Hungarian abbreviation: OTKA) under Grant No. NK100296 and the von Humboldt Foundation.

References

[1] Uijttewaal WSJ. The flow in groyne fields. In: Czernuszenko W, Rowinski P, editors. Water quality hazards and dispersion of pollutants. US: Springer; 2005. p. 231–46. http://dx.doi.org/10.1007/0-387-23322-9_12.
[2] Hentschel B, Anlauf A. Ecological optimization of groynes in the Elbe river. In: van Mazijk A, Weitbrecht V, editors. New insights in the physical and ecological processes in groyne fields, Delft; 2002. p. 121–133.
[3] Uijttewaal WSJ. Effects of groyne layout on the flow in groyne fields: Laboratory experiments. J Hydraul Eng 2005;131(9):782–91. http://dx.doi.org/10.1061/(ASCE)0733-9429(2005) 131:9(782).
[4] Van Mazijk A. Modelling the effects of groyne fields on the transport of dissolved matter within the Rhine Alarm-model. J Hydrol 2002;264(1):213–29. http://dx.doi.org/10.1016/S0022-1694(02)00077-X.
[5] Weitbrecht V, Uijttewaal WSJ, Jirka GH. A random walk approach for investigating near-and far-field transport phenomena in rivers with groin fields. Proc River Flow Naples 2004;2:1157–66.
[6] Engelhardt C, Krüger A, Sukhodolov A, Nicklisch A. A study of phytoplankton spatial distributions, flow structure and characteristics of mixing in a river reach with groynes. J Plankton Res 2004;26(11):1351–66. http://dx.doi.org/10.1093/plankt/fbh125.
[7] Bradshaw P, editor. Turbulence, topics in applied physics. Berlin, Heidelberg, New York: Springer-Verlag; 1976. Vol. 12.
[8] Prants SV, Budyansky MV, Ponomarev VI, Yu Uleysky M. Lagrangian study of transport and mixing in a mesoscale eddy street. Ocean Model 2011;38(1):114–25. http://dx.doi.org/10.1016/j.ocemod.2011.02.008.
[9] Haszpra T, Tél T. Volcanic ash in the free atmosphere: a dynamical systems approach. J. Phys. Conf. Ser. 2011;333(1–12):012008. http://dx.doi.org/10.1088/1742-6596/333/1/012008.
[10] Aref H. Stirring by chaotic advection. J Fluid Mech 1984;143(1):1–21. http://dx.doi.org/10.1017/S0022112084001233.
[11] Jung C, Tél T, Ziemniak E. Application of scattering chaos to particle transport in a hydrodynamical flow. Chaos Interdisciplinary J Nonlinear Sci 1993;3(4):555–68. http://dx.doi.org/10.1063/1.165960.
[12] Jacobs J, Ott E, Antonsen T, Yorke J. Modeling fractal entrainment sets of tracers advected by chaotic temporally irregular fluid flows using random maps. Physica D Nonlinear Phenom 1997;110(1):1–17. http://dx.doi.org/10.1016/S0167-2789(97)00122-X.
[13] Neufeld Z, Tél T. Advection in chaotically time-dependent open flows. Phys Rev E 1998;57(3):2832–42. http://dx.doi.org/10.1103/PhysRevE.57.2832.
[14] Lee WK, Taylor PH, Borthwick AGL, Chuenkhum S. Vortex-induced chaotic mixing in wavy channels. J Fluid Mech 2010;654:501–38. http://dx.doi.org/10.1017/S0022112010000674.
[15] Ottino JM. New applications of chaos in chemical engineering: intuition versus prediction. In: Kim JH, Stringer J, editors. Applied chaos. New York: John Wiley and Sons; 1992. p. 143–74.
[16] Ottino JM. The kinematics of mixing: stretching, chaos and transport. Cambridge: Cambridge University Press; 1989.
[17] Zsugyel M, Szabó KG, Kiss MZ, Józsa J, Ciraolo G, Nasello C, Tél T. Detecting the chaotic nature of advection in complex river flows. Periodica Polytech Civil Eng 2012;56(1):97–106. http://dx.doi.org/10.3311/pp.ci.2012-1.11.
[18] Sukhodolov AN, Uijttewaal WSJ, Schnauder I, Sukhodolova TA, Erdbrink C, Brevis W, et al. Quantitative visual methods for natural streams: examples and perspectives. Proc Congr Int Assoc Hydraul Res 2007;32(1):68.
[19] Ott E. Chaos in dynamical systems. Cambridge University Press; 1993.
[20] van Prooijen BC, Uijttewaal WSJ. A linear approach for the evolution of coherent structures in shallow mixing layers. Phys Fluids 2002;14(12). http://dx.doi.org/10.1063/1.1514660.
[21] Sokoray-Varga B, Józsa J. Particle tracking velocimetry (PTV) and its application to analyse free surface flows in laboratory scale models. Periodica Polytech Civil Eng 2008;52(2):63–71. http://dx.doi.org/10.3311/pp.ci.2008-2.02.
[22] Yu X, Tang X, Wang W, Wang F, Chen Z, Shi X. A lattice Boltzmann model coupled with a large eddy simulation model for flows around a groyne. Int J Sediment Res 2010;25:271–82. http://dx.doi.org/10.1016/S1001-6279(10)60044-3.
[23] Lai Y, Tél T. Transient chaos: complex dynamics on finite-time scales. Applied Mathematical Sciences, vol. 173. Springer; 2011. http://dx.doi.org/10.1007/978-1-4419-6987-3.
[24] Romeiras FJ, Grebogi C, Ott E. Multifractal properties of snapshot attractors of random maps. Phys Rev A 1990;41(2):784–99. http://dx.doi.org/10.1103/PhysRevA.41.784.
[25] Sommerer JC, Ott E. Particles floating on a moving fluid: a dynamically comprehensible physical fractal. Science 1993;259(5093):335–9. http://dx.doi.org/10.1126/science.259.5093.335.
[26] Tél T, Gruiz M. Chaotic dynamics. Cambridge: Cambridge University Press; 2006.
[27] Aurell E, Boffetta G, Crisanti A, Paladin G, Vulpiani A. Predictability in the large: an extension of the concept of Lyapunov exponent. J Phys A Math Gen 1997;30(1):1–26. http://dx.doi.org/10.1088/0305-4470/30/1/003.
[28] Cencini M, Cecconi F, Vulpiani A. Chaos: from simple models to complex systems, series on advances in statistical mechanics, vol. 17. World Scientific Publishing Company; 2010.
[29] Haller G, Yuan G. Lagrangian coherent structures and mixing in two-dimensional turbulence. Physica D 2000;147:352–70. http://dx.doi.org/10.1016/S0167-2789(00)00142-1.
[30] Haller G. Lagrangian coherent structures from approximate velocity data. Phys Fluids 2002;A14:1851–61. http://dx.doi.org/10.1063/1.1477449.
[31] Haller G. A variational theory of hyperbolic Lagrangian coherent structures. Physica D 2011;240:574–98. http://dx.doi.org/10.1016/j.physd.2010.11.010.
[32] Peacock T, Dabiri J. Introduction to Focus Issue: Lagrangian coherent structures. Chaos 2010;20:017501. http://dx.doi.org/10.1063/1.3278173.
[33] Peacock T, Haller G. Lagrangian coherent structures: the hidden skeleton of fluid flows. Phys Today 2013;66:41–7. http://dx.doi.org/10.1063/PT.3.1886.
[34] Karrasch D, Haller G. Do finite-size Lyapunov Exponents detect coherent structures? Chaos 2013;23:043126. http://dx.doi.org/10.1063/1.4837075.
[35] Uijttewaal WSJ, Lehmann D, van Mazijk A. Exchange processes between a river and its groyne fields: model experiments. J Hydraul Eng 2001;127(11):928–36. http://dx.doi.org/10.1061/(ASCE)0733-9429(2001) 127:11(928).
[36] <http://www.nature.com/news/2010/101011/full/news.2010.531.html>.